RSC Advances

ROYAL SOCIETY OF CHEMISTRY

www.rsc.org/advances

Graphical abstract
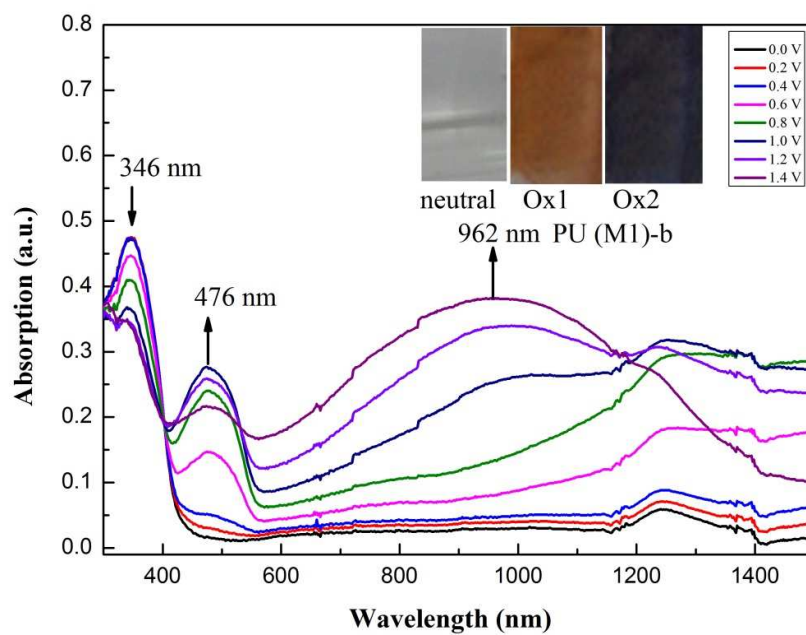
Electrochromic behaviors of PU (M1)-b thin film (in CH_3CN with 0.1 M $LiCO_4$ as the supporting electrolyte) at 0.0 V to 1.40 V (insets are the pictures of oxidized PU (M1)-b).

Polyurethanes Prepared from Isocyanates Containing Triphenylamine Derivatives: Synthesis and Optical, Electrochemical, Electrochromic and Memory Properties

Xiaotong Wu[a,1], Yanshuang Wu[b,1], Chunyu Zhang[a], Haijun Niu[a,*], Lei Lei[b,*], Chuanli Qin[a], Cheng Wang[a], Xuduo Bai[a], Wen Wang[c]

a *Key Laboratory of Functional Inorganic Material Chemistry, Ministry of Education; Department of Macromolecular Science and Engineering, School of Chemistry and Chemical Engineering, Heilongjiang University, Harbin 150086, P R China*

b *Department of Histology and Embryology, Harbin Medical University, Harbin,150081, Heilongjiang Province, China*

c *School of Material Science and Engineering, Harbin Institute of Technology, Harbin 150080, P R China*

*corresponding author, email: haijunniu@hotmail.com (Haijun Niu); leiys2002@yahoo.com (Lei Lei)

1. These authors contributed equally to this work

Abstract

Two novel series of triphenylamine (TPA)-containing aromatic polyurethanes (PUs) were synthesized via polymerization of N', N'-bis (α-naphthyl)-N, N'-bis (4-phenylisocyanate) biphenyl (M1) and N, N'-diphenyl-N, N'-bis (4-phenylisocyanate) biphenyl (M2) with different dihydroxy compounds. The structures of the polymers were characterized by Fourier Transform Infrared (FT-IR) spectroscopy, hydrogen nuclear magnetic resonance (^{1}H-NMR) and carbon nuclear magnetic resonance (^{13}C-NMR); and the thermostability and morphology were studied by

1

thermogravimetric analysis (TGA) and scanning electron microscope (SEM). The molecular

weights were measured to be from 1.02×10^4 to 1.31×10^4 by gel permeation chromatography

(GPC). The polymers were coated onto indium tin oxide (ITO) and the electrochromic properties

were investigated by using the ultraviolet visible (UV-vis) absorption spectra and cyclic

voltammetry (CV). The energy gaps were in the range of 2.21-2.26 eV. The polymer films

revealed good stability of the electrochromic characteristics by continuous cyclic scans, with a

color changing from neutral yellowish to a blue doped form at applied potentials. Meanwhile, PUs

film exhibited non-volatile write-once-read-many-times (WORM) memory behavior in the device

resulting from the non-isolated donor–acceptor (D–A).

Keywords: polyurethane; triphenylamine; electrochromic; cyclic voltammetry; memory behavior

Introduction

Electrochromism is known as the alternation of color by the application of a potential. [1] As

eletrochromic materials, conducting polymers (CPs) have attracted scientists' attention because of

their outstanding advantages over transition metal oxides, such as long-term stability, high

contrast ratio and coloration efficiency (CE), fast response time, low switching potential, and the

ease of color control through structure modification. [2-5] Of the available electrochromic CPs, in

particular, poly (3, 4-ethylenedioxythiophene) (PEDOT), polyaniline (PANI), polyfluorenes, poly

(3, 4-ethylenedithiathiophene) (PEDTT) and polyselenophenes, have also been extensively

investigated due to their unique electronic, redox properties, stable and multicolor behaviors. [3, 6–14] However, because of planar backbones and strong interaction of molecules, most CPs are

difficult to melt or be soluble to be processed. In order to expand the application of the polymers,

the researchers used many methods to increase the solubility of electroactive polymers such as by

introducing long alkyl or side groups. [15] Besides, introducing propeller-like TPA group into the polymers is one effective approach to improve solubility without sacrificing thermostability. [3] TPA and its derivatives, which have good ability of hole-transport, could also be used as electron donor, electrochromic materials and memory device. [16] The polymers based on TPA as core exhibit stable, excellent, multicolor, electrochromic and memory characteristic, furthermore the corporation of electron-donating substituents at the para positions of TPA affords stable radical cations. From 2005, Liou and Hsiao's groups have been researching deeply on a series of TPA-based polyimides, polyamide as electro-active layer in the field of electrochromic and memory device. [3, 16 17] Iwan and Skene group synthesized and investigated a series of aromatic polyazomethines with attractive optic-electronic properties and with low optical band gaps (1.3-2.0 eV) bearing TPA. [18-20] Our group has also systematically investigated the electrochemical, optical and electrochromic properties of polymers and composite with TPA derivatives. [21-23]

On the other hand, polyurethanes (PUs) form an important family of industrial polymers that have been widely used due to their good properties such as elasticity, flexibility, thermal stability, and excellent chemical resistance. [24–29] PU is one of the most versatile polymeric materials with regard to both processing methods and mechanical properties. [30] It can be found in almost every aspect of our lives, such as adhesives, in flexible foams, covers, fibers, medical devices and tissue scaffolds. [31-34] In recent decades, the research on photoelectric properties of PU has attracted intensively widespread attention. PU has been used in optical devices due to its good optical properties and processibility. [35-39] For example, PUs were used as effective hole-transport matrix [40-43] as well as light emitting layers. [44–46] PUs were reported with better thermal stability, band gap below 2.0 eV, non-linear optical, electrochemical properties, application in solar cell and ion sensor. [45, 47-49]

Zhang reported a new family of PUs with double-ended photo-cross-linkable groups and spindle-type chromophores. The cross-linked films displayed a high electro-optic coefficient up to 41 pm/V. [50] Peng has synthesized successfully electroactive PU containing trimer of amino aniline structure, and found that the electroactive PU had good corrosion resistance performance through a series of electrochemical corrosion test. [51] Yang has introduced WO_3 into PU materials to improve PU materials electrochromic performance. [52] Most investigation is focused on the PU made from toluene-2, 4-diisocyanate (TDI) or 4, 4'-diphenyl methane-diisocyanate (MDI). In this paper, we used triphosgene to prepare isocyanate which is facile and environmental-friendly to obtain, to the best of our knowledge, there is little research on electrochromic and memory properties study of PU prepared from isocyanate containing TPA.[22] In order to distinguish the difference between naphthyl and benzene, and understand the influence of different bisphenol structures on the properties of PUs, we reported two series of TPA-containing aromatic PUs based on the reaction of N,N'-bis (α-naphthyl)-N,N'-bis (4-phenylisocyanate) biphenyl (M1) and N,N'-diphenyl-N,N'-bis (4-phenylisocyanate) biphenyl (M2) with double hydroxyl compounds: phenolphthalein (a), bisphenol A (b), 4,4′-dihydro-xybiphenyl (c), 4,4′-bishydroxybenzophenone (d) and bisphenolfluorene (e), respectively. The characterization of biphenylamine-containing PUs was carried out by means of FT-IR, ^{1}H-NMR, ^{13}C-NMR, TGA and SEM. The optical, electrochemical and electrochromic properties of the PUs films were also tested by UV-vis spectroscopy and CV. The structure and E_g have been calculated by using quantum chemical program. The trend of E_gs that was measured by electrochemical method is similar to that of theoretical values which was calculated by quantum chemistry method. The memory devices were prepared with configuring the ITO/polymer/Al, and the memory properties were investigated by

I–V measurements. Furthermore, the PUs not only provide a member of new electrochromic materials, but also give theoretical analysis for memory devices.

Experimental

Materials

Dimethyl sulfoxide (DMSO) (analytical reagent) (A.R.), N, N-dimethylformamide (DMF) (A.R.) and dichloroethane were used after standard drying method. 4-Fluoronitrobenzene (A.R.) was distilled before used. Reagent grade aromatic bisphenol monomers that include phenolphthalein (a), bisphenol A (b), 4,4'-dihydroxybiphenyl (c), 4,4'-bishydroxybenzophenone (d), bisphenolfluorene (e) were used as received. Lithium perchlorate ($LiClO_4$) was dried under vacuum at 120 ^{o}C for 48 h. All the chemicals were purchased from Shanghai Sinopharm Co and TCI. N,N'-Bis(α-naphthyl)-4,4'-biphenyldiamine ($C_{32}H_{24}N_2$) (1) and N,N'-diphenyl-4, 4'-biphenyldiamine ($C_{24}H_{20}N_2$) (1') were used as received. The intermediate such as N, N'**-**bis (α-naphthyl)-N,N'-bis(4-aminophenyl)-4,4'-biphenyldiamine ($C_{44}H_{34}N_4$) (3) and N,N'-diphenyl-N, N'-bis(4-aminophenyl)-4,4'-biphenyldiamine ($C_{36}H_{30}N_4$) (3') and monomers M1, M2 were synthesized according to the modified method of references. [22, 53]

Synthesis of Monomers

The synthesis routes of M1 and M2 were outlined in Scheme S1.

M1 was synthesized by following the procedure. A solution of triphosgene (0.3472 g, 1.170 mmol) and dried dichloroethane (10 ml) were stirred at room temperature under N_2, and then was added dropwisely to a stirred solution of compound 3 (0.5450 g, 0.833 mmol). The final solution was heated 100 ^{o}C for 8 h under stirring. The obtained compound (M1) was collected by filtration and washed with petroleum ether, subsequently, the solvent was evaporated in vacuum, resulting in

0.4650 g of a light blue solid (yield: 59.4%). The monomer M2 was also synthesized via the same

synthesis route of the M1, except for the diamine reactant of

N,N'-diphenyl-N,N'-bis(4-aminophenyl)-4,4'-biphenyldiamine and 0.5478 g of a light blue solid

product (yield: 57.7%). M1 and M2 were characterized by FT-IR and ^{1}H-NMR and ^{13}C-NMR in

supporting information.

Synthesis of PUs

M1 (0.5035 g, 0.513 mmol) and dihydroxy phenolphthalein (0.2532 g, 0.892 mmol) being

dissolved in dry dichloroethane (10 ml) were put into a 50 mL, three-neck, round-bottom flask

under nitrogen atmosphere. The mixture was stirred at 70 °C for 24 h, yielding a dark viscous

solution. The obtained polymer was named of PU (M1)-a and was collected by filtration, resulting

in 0.2321 g of a dark solid (yield: 36.3%). Other PUs were also synthesized via the same synthesis

route of the PUs (M1)-a as shown in Scheme 1. The formation of PUs was confirmed by FT-IR,

^{1}H NMR and ^{13}C NMR spectroscopy in supporting information.

Scheme 1 Synthesis routes of PUs.

Preparation of film electrode

A polymer solution was made by dissolving about 0.02 g of the PU sample in 0.5 ml of DMF. The

resulting solution was cast on an ITO-coated glass, which was placed in the oven in vacuum

overnight for slow release of the solvent. Then thermally cured films were obtained by

programmed increasing temperature to 100 °C at heating rate of 10 °C/min and keeping the

temperature for 2 h. We controlled the concentration of the solution and casting speed at the same

level in order to keep the same thickness of different PUs. The obtained films were used for

thermal performance test, optical analyses and electrochemical test.

Fabrication and measurement of the memory device

The memory behaviors of these PUs were described by the current–voltage (I–V) characteristics of an ITO/polymer/Al sandwich device as shown in Fig. 1. The ITO glass and polymer film the memory device were the same above film electrode. The film thickness was determined to be around 50 nm. Finally, a 300 nm-thick Al top electrode was thermally evaporated through the shadow mask (recorded device units of 0.4×0.4 mm^2 in size) at a pressure of 10^{-7} Torr with a depositing rate of 3–5 Å s^{-1}. The electrical characterization of the memory device was performed by a Keithley 4200-SCS semiconductor parameter analyzer . Al was used as the anode during the voltage sweep, and ITO was set as the cathode.

Fig. 1 Molecular structures of PUs (M1) and PUs (M2) and a schematic diagram of the memory device consisting of a polymer thin film sandwiched between an ITO bottom electrode and an Al top electrode.

Measurements

FT-IR spectra were recorded on a PerkinElmer Spectrum 100 Model FT-IR spectrometer. ^{1}H and ^{13}C NMR spectra were measured on a Bruker AC-400 and AC-100 MHz spectrometer using DMSO-d$_6$. TGA was conducted on a PerkinElmer Pyris 6. The experiments were carried out by keeping about 6-8 mg powder samples heated in flowing nitrogen (flow rate = 20 cm^3/min) at a heating rate of 10 °C/min. SEM measurement was determined on an S4800 instrument with an accelerating voltage of 20 kV. The thickness of PU films (50 nm) coated ITO glass were carried out on profilometer XP-100 (Ambios Technology Inc.). Density-functional theory (DFT)

7

calculations were carried out using the B3LYP functional as implemented in Gaussian 98 program.

GPC analysis was performed on a Malvern instrument connected with one refractive index

detector (Viscotek-VE3580-RI- DETECTOR) at a flow rate of 0.8 ml/min at 35 $^{\circ}$C using DMF

solution and calibrated with polystyrene standard. UV-Vis spectra of the polymer films were

determined on a SHIMADZU UV-3600 spectrophotometer whereas the photoluminescence (PL)

solution spectra were registered on a Jasco FP-6200 spectrometer. The cyclic voltammograms

(CVs) were conducted on a CH Instruments 660A electrochemical analyzer with the use of a

three-electrode cell in which a platinum wire was used as an auxiliary electrode against a

home-made Ag/AgCl reference electrode and ITO was as a working electrode at a scan rate of 50

mV/s with a 0.1 M solution of $LiClO_4$ as an electrolyte under nitrogen atmosphere in dried

acetonitrile (CH_3CN), and calibrated against the ferrocene /ferrocenium (Fc/Fc^+) redox couple.

The memory behaviors of polymer were performed by a Keithley 4200-SCS semiconductor

parameter analyzer equipped.

Results and Discussion

FT-IR analysis and ^{1}H and ^{13}C NMR

Fig. S1 shows typical FT-IR spectra of M1 and PUs (M1). The distinct characteristic absorption of

M1 appears around 2261 cm^{-1}, which confirms the existence of -NCO group. After polymerization,

the absorption peak around 2261 cm^{-1} representing -NCO disappears, which shows the reaction

was completed. The characteristic peaks of urethane group of PUs (M1) are observed at 3230 cm^{-1},

1658 cm^{-1} and 1275 cm^{-1} corresponding to stretching vibrations of N-H, C=O and C-N-H groups,

respectively. FT-IR spectra of M2 and PUs (M2) are also shown in Fig. S1 in supporting

information. ^{1}H NMR and ^{13}C NMR spectra of PU (M1)-b in DMSO-d$_6$ are shown in Fig. 2.

^{1}H-NMR spectra of PU (M1)-b confirms that the peak at 7.95 is representing the hydrogen in NH-COO group and peak at 1.67 is representing the hydrogen in -CH₃. ^{13}C NMR spectra of PU (M1)-b show the signal at 152.2 corresponding to the ester carbonyl carbon and the singlet at 31.2 due to the -CH₃ carbons. All the detected peaks and ratios between the peak areas have been readily assigned to the carbon and hydrogen atoms of the PUs. ^{1}H NMR spectra and ^{13}C NMR spectra of the other PUs in DMSO-d_6 are shown in Fig. S2 in supporting information.

Fig. 2 ^{1}H and ^{13}C NMR spectra of PU (M1)-b in DMSO-d_6.

Polymer Film Morphologies, Thermal Stability and Molecular Weights

The morphologies of PU (M1)-a, PU (M1)-d and PU (M2)-a, PU (M2)-d are displayed by SEM in Fig. 3 and the morphologies of the other PUs are shown in Fig. S3. All the original PUs exhibit that the morphologies of the polymers are smooth, which means the morphologies are dependent on the chemical structures of PUs under the same conditions such as concentration, solvent and temperature. The morphology should be controlled to minimize the diffusion distance in PU film in order to achieve sufficient speed of charge. SEM images of PUs suggest the film would provide more ion channel and more reaction surface which makes it facile to transport counter ions.

The thermal properties of the PUs were investigated by TGA. Typical TGA curves of representative PU (M1)-b and PU (M2)-b in nitrogen atmospheres are shown in Fig. 4 and the other curves obtained in nitrogen atmospheres are shown in Fig. S4. The 10% and 60% weight-loss temperatures of these PUs in nitrogen were recorded in the range of 220-270 ^{o}C and 317-432 ^{o}C, respectively. The amount of carbonized residue (char yield) of these PUs in nitrogen atmosphere was more than 40% at 700 ^{o}C. Seen from Fig. 4, and the char yield of PU (M1)-b was

9

superior to PUs (M2)-b. It means that the high char yields of these polymers can be ascribed to their high aromatic content and the bulky naphthylamine-containing chromophores are more effective to preserve the thermal stability in the obtained PUs. Hence, high-temperature stability of the PUs could meet the requirements for optoelectronic thin-layer devices.

The number-average molecular weight ($\overline{M_n}$), polydispersity (PDI) and the average degree of polymerization (n) of PUs (M1) and PUs (M2) were determined to be in the range of 10,400-12,500, 1.06-1.49 and 10-14, 10,200-13,100, 1.04-1.57 and 11-14, respectively. (summarized in Table S1). The $\overline{M_n}$ and n indicates that the PUs (M1) containing α-naphthyl and PUs (M2) containing biphenyl groups have come into being.

Fig. 3 SEM images of PU (M1)-a, PU (M1)-d and PU (M2)-a, PU (M2)-d.

Fig. 4 TGA thermograms of PU (M1)-b and PU (M2)-b at a scan rate of 10 °C/min.

Optical properties

The optical properties of the PUs both in solution and in solid state were investigated by UV-vis spectroscopy and PL spectroscopy. In solid films, these PUs exhibited strong UV-Vis absorption bands in the range of 476-480 nm for PU (M1) and 480 nm-484 nm for PU (M2), respectively. Fig. 5 illustrates the strong UV-vis absorption bands PUs (M1) in the range of 345-349 nm in DMSO solution. It can be explained by the π-π* transitions resulting from charge transfer between nitrogen atoms from TPA units and the aromatic rings. The DMSO solution of the PUs (M1) were almost colorless and gave a green PL under irradiation with a general UV lamp (λ = 365 nm).

Their PL spectra in dilute DMSO solution (conc.: 10^{-8} M) showed maximum bands around 500-505 nm with little shift as also shown in Fig. 5. UV-vis absorption and PL spectroscopy of PUs (M2) are displayed in Fig. S5. PL quantum yields ϕs of the samples in DMSO solvents were measured by using quinine sulfate dissolved in 0.5 M sulfuric acids as reference standard (ϕ = 0.546). The ϕs of these PUs after refractive index correction can be calculated according to the following equation. [54]

$$\phi_{unk} = \phi_{std} \left(\frac{I_{unk}}{I_{std}} \right) \left(\frac{A_{std}}{A_{unk}} \right) \left(\frac{\eta_{unk}}{\eta_{std}} \right)^2$$

where ϕ_{unk}, ϕ_{std}, I_{unk}, I_{std}, A_{unk}, A_{std}, η_{unk} and η_{std}, are the fluorescent quantum yield, integration of the emission intensity, absorbance at the excitation wavelength, and the refractive indices of the corresponding solutions for the samples and the standard, respectively. The PL quantum yield of PUs in dilute DMSO solution ranges: 3.75% (PU (M1)-d) < 5.08% (PU (M1)-a) < 5.29% (PU (M1)-c) < 5.58% (PU (M1)-e) < 6.23 % (PU (M1)-b), 2.37% (PU (M2)-e) < 3.58% (PU (M2)-b) < 3.71% (PU (M2)-d) < 3.84% (PU (M2)-a) < 4.70% (PU (M2)-c). The quantum yield of PU (M1)-b measured in DMSO is the highest among two series of polymers. PUs (M1) containing α-naphthyl show the higher quantum yield than PUs (M2) containing biphenyl groups due to that naphthyl have more conjugated structrure. The quantum yield of PU (M1)-b and PU (M2)-c measured in DMSO is the highest among PUs (M1) and PUs (M2) series, respectively. This may be the result of the better electron-donating capability of methyl (-CH$_3$) substituent in the bisphenol A of PU (M1)-b and bisphenolfluorene groups with more planar would contribute more to the emission of PUs than the other groups.

Fig. 5 UV-vis absorption and PL spectra of PUs (M1) with a concentration of DMSO (conc.: 10^{-8} M). PL photos of PUs in DMSO solution (10^{-8} M) by UV irradiation at 365 nm being inset.

11

Electrochemical properties

The electrochemical properties of the PUs were investigated by CV. The CVs exhibited two reversible oxidation redox couples for PUs (M1) and one reversible oxidation redox couple for PUs (M2). The color of PUs films changed from yellowish to blue during the electrochemical oxidation of the thin PUs films. The Fc/Fc$^+$ couple was used to calculate the half-wave potentials ($E^{Fc/Fc+}_{1/2}$, 0.40 V) vs Ag/AgCl in CH$_3$CN in order to obtain accurate reoxidation potential. The typical CVs for PU (M1)-a and PU (M2)-a are shown in Fig. 6, and CVs of the other PUs are displayed in Fig. S6. PU (M1)-a and PU (M2)-a exhibited two reversible oxidation redox couples with $E_{1/2}^{1}$ = 0.69 V vs Ag/AgCl, $E_{1/2}^{2}$ = 0.91 V vs Ag/AgCl and with $E_{1/2}^{1}$ = 0.65 V vs Ag/AgCl, $E_{1/2}^{2}$ = 0.87 V vs Ag/AgCl, respectively. Each peak is attributed to one electron removal from the nitrogen atom at TPA structure in each repeating unit to yield a stable delocalized radical cation [55]. The first peak (at 0.78 and 0.80 V vs Ag/AgCl) can be attributed to oxidation of the electron-rich nitrogen atom in one of the TPA groups. The second peak (at 1.02 V and 1.02 V vs Ag/AgCl) can be ascribed to the generation of the dication from radical cation which would cause the radical recombination and formation of a quinoid structure. In addition, the PU (M2)-a had lower reduction potentials than PU (M1)-a due to the latter having a stronger electron withdrawing action of naphthyl group. The energy of the highest occupied molecular orbital (HOMO) and lowest unoccupied molecular orbital (LUMO) levels of the investigated PUs can be determined from the onset oxidation potentials and the onset absorption wavelength which are summarized in Table 1. Assuming that the energy level for the Fc/Fc$^+$ standard is 4.80 eV with respect to the zero vacuum level, the HOMO energy values for PUs are calculated using the equation: [23]

$$E_{HOMO} = - (E_{OX} \text{ vs Ag/AgCl} + 4.4) \text{ eV}$$

where E_{OX} is the onset oxidation potential. E_{HOMO}s of PUs (M1) and PUs (M2) are calculated to be

at in the range from -5.02 to -5.03 eV and from -4.99 to -5.07 eV, respectively. The LUMO energy

level values of the PUs are estimated from the HOMO energy level and E_g which could be

obtained as following:

$$E_{LUMO} = E_{HOMO} + E_g$$

$$E_g = 1240 / \lambda_{onset}$$

E_{LUMO}s and E_g are calculated to be at in the range from at -2.77 eV to -2.78 eV and 2.78 eV to 2.82

eV, respectively. The low-lying HOMO energy level of these polymers suggest that they have

potential for use as hole-transporting and blue light-emitting materials in emitting devices. In

Table 1, we can see that two series of PUs do not exhibit significant difference in electrochemical

properties (E_{HOMO} values, E_{LUMO} values and E_g). It is because the onset oxidation potential is very

similar between 0.56 V and 0.64 V due to the influence of similar TPA structures, same

experimental conditions and the PDI of molecular weight of PUs. From table 1, we observed PUs

(M2) series had the smaller E_g values because that the pendent naphthyl group is a more

conjugated structure and stronger polarity group than benzene group, and the electron transfer of

the series of PUs (M1) would need more energy than that of PUs (M2) from the HOMO orbital to

LUMO orbital. Seen from the Fig 6, the peaks of reoxidation are different which is ascribed to

difference of polarities of bezene and naphthyl group. Thus, the novel PUs can be used as

potential candidates in dynamic electrochromic screen devices due to their suitable thermal

stabilities, E_{HOMO} values and reversible electrochemical behaviors.

Fig. 6 CVs of (a) ferrocene (b) PU (M1)-a (c) PU (M2)-a films onto an ITO-coated glass substrate

in 0.1 M LiClO$_4$/CH$_3$CN at the scanning rate of 50 mV/s.

Table1 Optical and electrochemical properties of the PUs.

Quantum chemical calculation

The ground-state geometries of the PUs were optimized by hybrid density functional theory

(B3LYP) with 6-31 G basis set, and are presented in Fig. 7 and Fig. S7. E_{HOMO} often expresses

the ability of electron donating, and E_{LUMO} often associates with the ability of accepting

electrons. [56] The HOMO and LUMO energies and their energy gaps ($E_{\mathrm{g}}^{\mathrm{quntum}}$) are given in Table 1.

The electronic wave function of the HOMO is distributed throughout TPA part of PUs, which is

good to get higher hole mobility. The electronic wave function of the LUMO is mainly localized

on the dihydroxy portion. The trend of E_{g} for the series of PUs follows in the order: PUs (M2) <

PUs (M1) in Table 1. The measured data have a slight deviation compared with the theoretical

data due to the affection of the molecular interaction, molecular structure and solvation process.

The results show that the naphthyl group with more polarity and the different bisphenol derivative

structures play the key role in regulating the gaps of PUs altogether.

Fig. 7 Pictorial representations of the electron density in the frontier molecular orbitals of

repetition units for PUs (M1).

Electrochromic properties

Electrochromic absorption spectra these PUs thin films were examined by a UV–vis spectrometer

at different applied potentials, and electrochromism was monitored by casting polymer solution

onto an ITO-coated glass substrate. Solution conditions and the electrode preparations were

identical to those applied in CV experiments. All these PUs showed similar electrochromic properties, and the typical electrochromic absorbance spectra of PU (M1)-b and PU (M2)-b are illustrated in Fig. 8. In the neutral form, the PU (M1)-b exhibited strong absorption at 346 nm at 0 V due to characteristic of π-π* transitions in TPA. In this oxidized state, PU (M1)-b has two absorption peaks at 346 nm and 476 nm due to the first stage oxidation. When the applied potential increased from 0.6 to 1.4 V, corresponding to the second step oxidation, the peak of absorption at 346 nm decreased gradually, while new band grew up at 962 nm, and the peak of absorption wavelength at 476 nm increased gradually in intensity. For PU (M2)-b, when the applied potentials were adjusted positively from 0.0 to 1.4 V, the peak of absorption at 354 nm decreased gradually for neutral form, while two new bands grew up at 480 and 908 nm, respectively. Meanwhile, the film of PU (M1)-b and PU (M2)-b changed from original colorless to yellow and then to a blue oxidized form. Similar spectral changes for other PUs of PUs (M1) series and the corresponding PUs (M2) series were observed in Fig. S8. The spectral changes in visible range are assigned to the formation of a stable cationic radical of the TPA center in moiety. Furthermore, the broad absorption in NIR region is the characteristic result due to intervalence-charge transfer (IV-CT) excitation associated with electron transfer (ET) from active neutral nitrogen atom to the cation radical nitrogen center of PUs, which is consistent with the phenomenon classified by Robin and Day. [57]

Fig. 8 Electrochromic behaviors of PU (M1)-b and PU (M2)-b thin film (in CH_3CN with 0.1 M $LiCO_4$ as the supporting electrolyte) at 0.0 V to 1.40 V (insets are the pictures of oxidized PU (M1)-b and PU (M2)-b).

15

Electrochromic Switching

Optical switching processes were further investigated in order to clarify the electrochromic characteristics of these novel PUs. Polymers were cast on ITO-coated glass slides in the same manner as described above, then chronoamperometric and absorbance measurements were performed at the same time. When the voltage was switched, the absorbance at the given wavelength was monitored as a function of time with UV-vis-NIR spectroscopy. The color switching time was estimated by applying a potential step, and the absorbance profile was followed. The switching time was defined as the time required for reach 90% of the full change in absorbance after the switching of the potential. Thin film of PU (M1)-b required 1.0 s at 0.8 V for switching absorbance at 476 nm and 1.0 s for bleaching. The color switching cycles of PU (M1)-b and PU (M2)-b are shown in Fig. 9. After over continuous 300 continuous cyclic switches between 0.0 and 0.8 V in 3000 s, the polymer films still exhibited good stability of electrochromic characteristics. Thin film of PU (M2)-b exhibited same manner as PU (M1)-b. Similar electrochromic switching for the other PUs of PUs (M1) series and the PUs (M2) series were observed in Fig. S9, and also exhibited good stability of electrochromic characteristics. The electrochromic coloration efficiency (CE; η) is also an important characteristic for the electrochromic materials. CE can be calculated using the equations and given below: [58]

$$\delta_{OD} = lg(T_b/T_c)$$

$$\eta = \delta_{OD}/Q$$

Where T_b and T_c are the transmittances before and after coloration, respectively, δ_{OD} is the change of the optical density, which is proportional to the amount of created color centers. η denotes the CE (cm^2/C) and Q (mC/cm^2) is the amount of injected/ejected charge per unit sample area. The

electrochromic CEs of PU films are summarized in Table S2. PUs (M2) containing biphenyl groups show the higher CE than PUs (M1) containing α-naphthyl. The reason is that PU containing biphenyl groups has the more facile CT, which plays the key role in the CEs. PU (M1)-a and PU (M2)-e exhibited the highest CE of the PUs (M1) and PUs (M2), respectively, which were maybe attributed to that phenolphthalein or bisphenolfluorene structures and facile solvation process.

Fig. 9 Optical switching procedures (0.1 M LiClO$_4$ as the supporting electrolyte with a cycle time of 10 s): (a) potential step transmittance and (b) Current consumption of PU (M1)-b and PU (M2)-b at 480 nm.

Memory device characteristics

The memory behaviors of these PUs were described by the I–V characteristics of an ITO/polymer/Al sandwich device as shown in Fig. 10. Within the sandwich device, polymer film was used as an active layer between Al and ITO as the top and bottom electrodes. All polymer films standard thickness were coated as 50 nm in order to exclude the effect of the polymer film thickness on memory properties. Fig. 10 (a) depicts the I-V results of PU (M1)-b. During the first positive sweep from 0V to 3V, the device based on PU (M1)-b could not be switched to the ON state and stayed in the OFF state with a current range 10^{-8} to 10^{-4}A. However, the current increases abruptly from 10^{-4} to 10^{-1} A (high-conductivity state) at the threshold voltage of 3.0 V during the positive sweep, indicating that the device undergoes an electrical transition from the OFF state to the ON (high-conductivity) state (writing process). In a memory device, this OFF-to-ON transition can be defined as a "writing" process. The device remained at the ON state during the subsequent positive scan (the second sweep) and then negative scan (the third sweep). The PU (M1)-b

17

memory device also remained in the ON state during the subsequent positive (the fourth sweep)

and negative scans (the fifth sweep) after turning off power for 10 min. These results indicate that

the PU (M1)-b films exhibit non-volatile write-once-read-many-times (WORM) memory behavior

in the device. Fig. 10b reveals the I–V result of PU (M2)-b, the current increasing from 10^{-8} to 10^{-5}

to 10^{-4} to 10^{-1} A (high-conductivity state) instantaneously at the threshold voltage of 2.9 V in the

first positive sweep (line 1), indicating the writing process for the transition from the OFF state to

the ON state. The device remained in the ON state during the subsequent positive scan (line 2) and

the subsequent negative scan (line 3) which could be defined as the reading process. After turning

off the power for 10 min, the memory device could be switched on again at threshold voltage 3.2

V (line 4), the PU (M2)-b memory device also remained in the ON state during the subsequent

positive scan (the fifth sweep). These results indicate that the PU (M2)-b films also exhibit

non-volatile WORM memory behavior in the device. The increased ON/OFF current ratio is

advantageous to reduce the probability of misreading between the ON state and the OFF state. [16]

Fig. 10 Curent-voltage (I-V) characteristics of the ITO/polymer (50nm)/Al memory device. (a) PU

(M1)-b, (b) PU (M2)-b.

Switching mechanism of the PUs (M1) and PUs (M2)

We could get more understanding of the memory behavior of the PUs (M1) and PUs (M2) devices

from Fig. 7 and Fig. S7. These two systems could proceed via a similar charge transfer route from

TPA donor to the acceptor due to their similar molecular orbital location. During the positive

voltage sweep, both PUs (M1) and PUs (M2), with analogous charge density distribution, proceed

via a similar charge transfer pathway from TPA donor to the acceptor as the applied potential

reaches the switching-on voltage. Some electrons at the HOMO may accumulate energy then overcome the band gap, thus transit to the LUMO resulting in an excited state. Therefore, charge transfer could occur from the HOMO to the LUMO to form conductive charge transfer complexes. In addition, during the intermolecular charge transfer induced by the applied electric field, the generating holes can be delocalized within TPA moieties resulting in a conducting channel in the polymer chain, which facilitate the migration of charge carriers (holes). The linkage between donor and acceptor in PUs can efficiently prevent the intramolecular backward route, thus stabilizing the CT complex.[16]

Conclusions

Two series of new TPA-based PUs had been successfully prepared for the first time for memory device applications. PUs displayed a good solubility in common solvents, which is good for polymer film-forming by the solution casting method. The results presented also showed that introducing bulky TPA group into polymer backbone maintained good thermal stability. All obtained PUs revealed good reversible electrochemical behavior, continuous cyclic stability of electrochromic characteristics and memory device characteristics. Thus, these novel TPA-containing PUs have many applications as light-emitting materials, hole-transporting materials, electrochromic materials and memory device application.

Acknowledgements

References

1 C. J. Yao, Y. W, Zhong, H. J. Nie, H. D. Abruna and J. Yao, *J. Am. Chem. Soc.*, 2011, **133**, 20720–20723.

2 S. M. Zhang, J. K. Xu, B. Y. Lu, L. Q. Qin, L. Zhang, S. J. Zhen and D. Mo, *J. P. Sci., Part A: polym. Chem.*, 2014, **52**, 1989–1999.

3 (a) H. M. Wang and S. H. Hsiao, *J. Polym. Sci. Part A: Polym. Chem.*, 2014, **52**, 1172–1184. (b) S. H. Hsiao, P. C. Chang, H. M. Wang, Y. R. Kung and T. M. Lee, *J. Polym. Sci. Part A: Polym. Chem.*, 2014, **52**, 825–838. (c) S. H. Hsiao, G. S. Liou, Y. C. Kung and T. J. Hsiung, *J. Polym. Sci. Part A: Polym. Chem.,* 2010, **48**, 1013–1023. (d) S. H. Hsiao, G. S. Liou Y. C. Kung and Y. M. Chang, *J. Polym. Sci. Part A: Polym. Chem.*, 2010, **48**, 1013–1023.

4 (a) H. Y. Qu, H. C. Zhang, N. Li, Z. Q. Tong, J. Wang, J. P. Zhao and Y. Li, *RSC Adv.*, 2015, **5**, 803–806. (b) Y. J. Tao, Y. J. Zhou, X. Q. Xu, Z. Y. Zhang, H. F. Cheng and W. W. Zheng, *Electrochim. Acta*, 2012, **78**, 353–358. (c) Pierre M. Beaujuge and John R. Reynolds, Chem. Rev., 2010, **110**, 268-320.

5 S. O. Hacioglu, S. Toksabay, M. Sendur and L. Toppare, *J. Polym. Sci. Part A: Polym. Chem.*, 2014, **52**, 537–544.

6 Y. S. Jeong and K. Akagi, *Macromolecules*, 2011, **44**, 2418–2426.

7 A. P. Saxena, M. Deepa, A. G. Joshi, S. Bhandari and A. K. Srivastava, *ACS Appl. Mater. Inter.*, 2011, **3**, 1115–1126.

8 G. Ćirić-Marjanović, *Synth. Met.*, 2013, **170**, 31–56.

9 F. M. Kelly, L. Meunier, C. Cochrane and V. Koncar, *Displays*, 2013, **34**, 1–7.

10 S. X. Xiong, F. Yang, G. Q. Ding, K. Y. Mya, J. Ma and X. H. Lu, *Electrochim. Acta*, 2012, **67**,

194–200.

11 S. M. Zhang, L. Q. Qin, B. Y. Lu and J. K. Xu. *Electrochim. Acta*, 2013, **90**, 452–460.

12 B. Y. Lu, S. M. Zhang, L. Q. Qina, S. Chen, S. J. Zhen and J. K. Xu, *Electrochim. Acta*, 2013, **106**, 201–208.

13 A. Patra and M. Bendikov, *J. Mater. Chem.*, 2010, **20**, 422–433.

14 S. S. Zade, N. Zamoshchik and M. Bendikov, *Acc. Chem. Res.*, 2011, **44**, 14–24.

15 L.T. Huang, H. J. Yen, G. S. Liou, *Macromolecules*, 2011, **44**, 9595–9610.

16 (a) L. J. Liu, Q. Guo, J. Y. Li, B. Yao and W. J. Tian, *Chinese J. Chem.*, 2013, **31**, 456–464. (b) C. J. Chen, Y. C. Hu and G. S. Liou, *Polym. Chem.*, 2013, **26**, 06. (c) Y. C. Hu, C. J. Chen, H. J. Yen, K. Y. Lin, J. M. Yeh, W. C. Chen and G. S. Liou, *J. Mater. Chem.*, 2012, **22**, 20394–20402. (d) C. J. Chen, H. J. Yen, W. C. Chen and G. S. Liou, *J. Mater. Chem.*, 2012, **22**, 14085–14093. (e) Y. Chen, C. L. Tan, H. Zhang and L. Z. Wang, *Chem. Soc. Rev.*, 2015, DOI: 10.1039/C4CS00300D. (f) Y. Chen, B. Zhang, G. Liu, X. D. Zhuang and E. T. Kang, *Chem. Soc. Rev.*, 2012, **41**, 4688–4707. (g) C. L. Tan, Z. D. Liu, W. Huang and H. Zhang, *Chem. Soc. Rev.*, 2015, DOI: 10.1039/c4cs00399c.

17 (a) S. H. Cheng, S. H. Hsiao, T. H. Su and G. S. Liou, *Macromolecules*, 2005, **38**, 307–316; (b) C. W. Chang, G. S. Liou and S. H. Hsiao, *J. Mater. Chem.*, 2007, **17**, 1007–1015; (c) H. J. Yen and G. S. Liou, *Chem. Mater.*, 2009, **21**, 4062–4070; (d) H. J. Yen, H. Y. Lin and G. S. Liou, *Chem. Mater.*, 2011, **23**, 1874–1882; (e) L. T. Huang, H. J. Yen and G. S. Liou, *Macromolecules*, 2011, **44**, 9595–9614; (f) H. J. Yen and G. S. Liou, *Polym. Chem.*, 2012, **3**, 255–264; (g) Y. W. Chuang, H. J. Yen and G. S. Liou, *Chem. Commun.*, 2013, **49**, 9812–9814.

18 D. Sek, A. Iwan, B. Jarzabek, B. Kaczmarczyk, J. Kasperczyk, Z. Mazurak, M. Domanski, K.

Karon and M. Lapkowski, *Macromolecules*, 2008, **41**, 6653–6663.

19 A. Bolduc, S. Dufresne and W.G. Skene, *J. Mater. Chem.*, 2010, **20**, 4820–4826.

20 L. Sicard, D. Navarathne, T. Skalski and W. G. Skene, *Adv. Funct. Mater.*, 2013, **23**, 3549–3559.

21 (a) L. N. Ma, H. J. Niu, J. W. Cai, P. Zhao, C. Wang, X. D. Bai, Y. F. Lian and W. Wang, *Carbon*, 2014, **67**, 488–499. (b) Y. Q. Wang, Y. Liang, J. Y. Zhu, X. D. Bai, X. K. Jiang, Q. Zhang and H. J. Niu, *RSC Adv.*, 2015, **5**, 11071–11076.

22 (a) C. Y. Zhang, Y. J. Hou, H. J. Niu, Y. F. Lian, X. D. Bai, C. Wang and W. Wang, *J. Electroanal. Chem.*, 2014, **717**, 165–171. (b)Vera Bllaert, Frans C, De Schryer, *Adv. mater.*, 1993, **5**, 268-270. (c) K. D. Belfield, O. Najjar and S. R. Sriram, *polymer*, 2000, **41**, 5011-5020.

23 K. Zhang, H. J. Niu, C. Wang, X. D. Bai, Y. F. Lian and W. Wang, *J. Electroanal. Chem.*, 2012, **682**, 101–109.

24 Y. Li, W. Kang, J. O. Stoffer and B. Chu, *Macromolecules*, 1994, **27**, 612–614.

25 K. I. Suresh and V. S. Kishanprasad, Ind. *Eng. Chem. Res.*, 2005, **44**, 4504–4512.

26 R. J. Green, S. Corneillie, J. Davies, M. C. Davies, C. J. Roberts, E. Schacht, S. J. B. Tendler and P. M. Williams, *Langmuir*, 2000, **16**, 2744–2750.

27 M. Hasegawa, T. Ikawa, M. Tsuchimori, O. Watanabe and Y. Kawata, *Macromolecules*, 2001, **34**, 7471–7476.

28 B. R. Crenshaw and C. Weder, *Macromolecules*, 2006, **39**, 9581–9589.

29 J. D. Tovar and C. P. Harvey, *J. Polym. Sci. Part A: Polym. Chem.*, 2011, **49**, 4861–4874.

30 Y. Lu and R. C. Larock, *Biomacromolecules*, 2008, **9**, 3332–3340.

31 O. G. Armagan, B. K. Kayaoglu, H. C. Karakas and F. S. Guner, *J. Ind. Textil.*, 2014, **43**, 396–414.

32 M. Sponton, N. Casis, P. Mazo, B. Raud, A. Simonetta, L. Rios and D. Estenoz, *Int. Biodeter. Biodegr.*, 2013, **85**, 85–94.

33 V. Jaso, J. Milic, V. Divjakovic and Z. S. Petrovic, *Eur. Polym. J.*, 2013, **49**, 3947–3955.

34 H. Y. Mi, X. Jing, M. R. Salick, T. M. Cordie, X. F. Peng and L. S. Turng, *J. Mater. Sci.*, 2014, **49**, 2324–2337.

35 M. Špírková, J. Pavličević, A. Strachota, R. Poreba, O. Bera, L. Kaprálková, J. Baldrian, M. Šlouf, N. Lazić and J. Budinski-Simendić, *Eur. Polym. J.*, 2011, **47**, 959–972.

36 K. Bagdi, K. Molnár, M. Kállay, P. Schön, J. G. Vancsó and B. Pukánszky, *Eur. Polym. J.*, 2012, **48**, 1854–1865.

37 L. Peponi, I. Navarro-Baena, A. Sonseca, E. Gimenez, A. Marcos-Fernandez and J. M. Kenny, *Eur. Polym. J.*, 2013, **49**, 893–903.

38 P. Russo, M. Lavorgna, F. Piscitelli, D. Acierno and L. D. Maio, *Eur. Polym. J.*, 2013, **49**, 379–388.

39 Z. S. Petrovic, D. P. Hong, I. Javni, N. Erina, F. Zhang and J. Ilavsky, *Polymer*, 2013. **54**, 372–380.

40 C. H. Kuo, K. C. Peng, L. C. Kuo, K. H. Yang, J. H. Lee, M. k. Leung and K. H. Hsieh, *Chem. Mater.*, 2006, **18**, 4121–4129.

41 C. H. Ku, C. H. Kuo, C. Y. Chen, M. k. Leung and K. H. Hsieh, *J. Mater. Chem.*, 2008, **18**, 1296–1301.

42 K. R. Lin, C. H. Kuo, L. C. Kuo, K. H. Yang, M. k. Leung and K. H. Hsieh, *Eur. Polym. J.*,

2007, **43**, 4279–4288.

43 C. N. Chuang, C. H. Kuo, Y. S. Cheng, C. K. Huang, M. k. Leung and K. H Hsieh, *Polymer*,

2012, **53**, 2001–2007.

44 H. Lim, J. Y. Noh, G. H. Lee, S. E. Lee, H. Jeong, K. Lee, M. Cha, H. Suh and C. S. Ha, *Thin*

Solid Films, 2000, **363**, 152–155.

45 H. Jeong, D. Zou, T. Tsutsui and C. S. Ha, *Thin Solid Films*, 2000, **363**, 279–281.

46 C. H. Ku, C.H. Kuo, M. k. Leung and K. H. Hsieh, *Eur. Polym. J.*, 2009, **45**, 1545–1553.

47 (a) İ. Kaya and M. Kamaci, *J. Appl. Polym. Sci.*, 2012, **125**, 876–887. (b) İ. Kaya and M.

Kamaci, *J. Inorg. Organomet. Polym.*, 2014, **24**, 803–818. (c) İ. Kaya and M. Kamaci, *Prog.*

Org. Coat., 2012, **74**, 204–214. (d) İ. Kaya and M. Kamaci, *J. Inorg. Organomet. Polym.*,

2013, **23**, 1159–1171. (e) İ. Kaya, M. Yildirim and M. Kamaci, *Synthetic Met.*, 2011, **161**,

2036–2040.

48 (a) N. P. Wang and T. M. Leslie, *Chem. Mater.*, 1996, **7**, 185-191; (b) I. Ali, S. M. Al-Zahrani

and S. K. Dolui, *Polym. Sci. Ser. B*, 2012, **54**, 342–348.

49 A, Shanavas, M. Vanjinathan, A. S. Nasar, S. Amudha and S. A.Suthanthiraraj, *High Perform.*

Polym., 2012, **24**, 561–570.

50 X. L. Zhang, M. Li, Z. S, Shi, R. L. Jin, X. B. Wang, Y. F. Yan, M. B. Yi, D. M. Zhang, and Z.

C. Cui, *J. Mater. Sci.*, 2011, **46**, 4458–4464.

51 C. W. Peng, C. Hsu and K. H. Lin, *Electrochim. Acta*, 2011, **58**, 614–620.

52 C. H. Yang, L. W. Chong and L. M. Huang, *Mater. Chem. Phys.*, 2005, **91**, 154–160.

53 W. Kuran, M. Sobczak, T. Listos, C. Debek and Z. Florjanczyk, *Polymer*, 2000, **41**,

5011–5020.

54 G. S. Liou, S. M. Lin and H. J. Yen, *Eur. Polym. J.*, 2008, **48**, 2608–2618.

55 G. S. Liou, N. K. Huang and Y. L. Yang, *J. Polym. Sci. Part A: Polym. Chem.*, 2006, **44**, 4095–4097.

56 A. A. Nazeer, N. K. Allam, A. S. Fouda and E. A. Ashour, *Mater. Chem. Phys.*, 2012, **136**, 1–9.

57 C. H. Duan, W. Z. Cai, F. Huang, J. Zhang, M. Wang and T. B. Yang, *Macromolecules*, 2010, **43**, 5262–5268.

58 S. J. Yoo, J. H. Cho, J. W. Lim, S. H. Park, J. Jang and Y. E. Sung, *Electrochem. Commun.*, 2010, **12**, 164–167.

Captions

Scheme 1 Synthesis routes of PUs.

Table1 Optical and electrochemical properties of the PUs.

Fig. 1 Molecular structures of PUs (M1) and PUs (M2) and a schematic diagram of the memory

device consisting of a polymer thin film sandwiched between an ITO bottom electrode and an Al

top electrode.

Fig. 2 ^{1}H and ^{13}C NMR spectra of PU (M1)-b in DMSO-d$_6$.

Fig. 3 SEM images of PU (M1)-a, PU (M1)-d and PU (M2)-a, PU (M2)-d.

Fig. 4 TGA thermograms of PU (M1)-b and PU (M2)-b at a scan rate of 10 ^{o}C/min.

Fig. 5 UV-vis absorption and PL spectra of PUs (M1) with a concentration of DMSO (conc.: 10^{-8}

M). PL photos of PUs in DMSO solution (10^{-8} M) by UV irradiation (Excited at 365 nm) being

inset).

Fig. 6 CVs of (a) ferrocene (b) PU (M1)-a (c) PU (M2)-a films onto an ITO-coated glass substrate

in 0.1 M LiClO$_4$/CH$_3$CN at the scanning rate of 50 mV/s.

Fig. 7 Pictorial representations of the electron density in the frontier molecular orbitals of

repetition units for PUs (M1).

Fig. 8 Electrochromic behaviors of PU (M1)-b and PU (M2)-b thin film (in CH$_3$CN with 0.1 M

LiCO$_4$ as the supporting electrolyte) at 0.0 V to 1.40 V (insets are the pictures of oxidized PU

(M1)-b and PU (M2)-b).

Fig. 9 Optical switching procedures (0.1 M LiClO$_4$ as the supporting electrolyte with a cycle time

of 10 s): (a) potential step transmittance and (b) Current consumption of PU (M1)-b and PU

(M2)-b at 480 nm.

Fig. 10 Curent-voltage (I-V) characteristics of the ITO/polymer (50nm)/Al memory device. (a) PU

(M1)-b, (b) PU (M2)-b.

Supporting information captions

Scheme S1 Synthesis routes of M1 and M2.

Table S1 Molecular weights of the PUs.

Table S2 Optical and Electrochemical Data Collected for Coloration Efficiency Measurements of

polymers.

Fig. S1 FT-IR spectra of M1, M2, PUs (M1) and PUs (M2).

Fig. S2 ^{1}H and ^{13}C NMR spectra of PUs (M1) and PUs (M2) in DMSO-d$_6$.

Fig. S3 SEM images of other PUs (M1) and PUs (M2).

Fig. S4 TGA thermograms of PUs (M1) and PUs (M2) at a scan rate of 10 ^{o}C/min.

Fig. S5 UV-vis absorption and PL spectra of PUs (M2) with a concentration of DMSO (conc.: 10^{-8}

M).

Fig. S6 CVs of PUs (M1) and PUs (M2) films onto an ITO-coated glass substrate in 0.1 M

LiClO$_4$/CH$_3$CN at the scanning rate of 50 mV/s.

Fig. S7 Pictorial representations of the electron density in the frontier molecular orbitals of

repetition units for PUs (M2).

Fig. S8 Electrochromic behaviors of PUs (M1) and PUs (M2) thin film in CH$_3$CN with 0.1 M

LiCO$_4$ as the supporting electrolyte (insets are the pictures of oxidized PUs).

Fig. S9 Optical switching procedures (0.1 M LiClO$_4$ as the supporting electrolyte with a cycle

time of 10 s): (a) potential step transmittance of PUs (M1) and PUs (M2) by applying a potential

step (0.0-0.8 V). (b) Current consumption of the other PUs (M1) and PUs (M2).
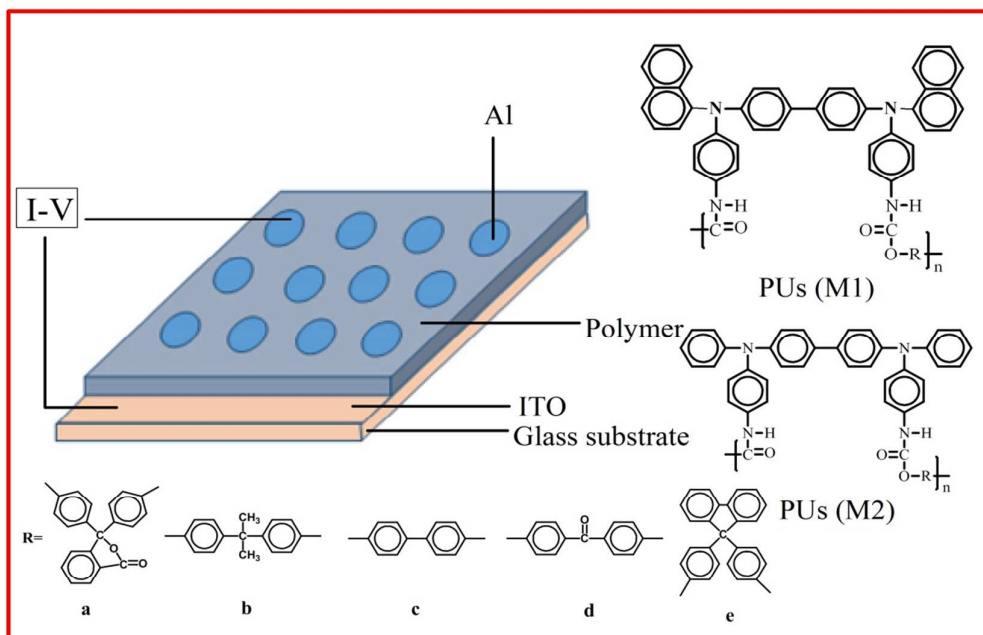
27

Fig. 1 Molecular structures of PUs (M1) and PUs (M2) and a schematic diagram of the memory

device consisting of a polymer thin film sandwiched between an ITO bottom electrode and an Al
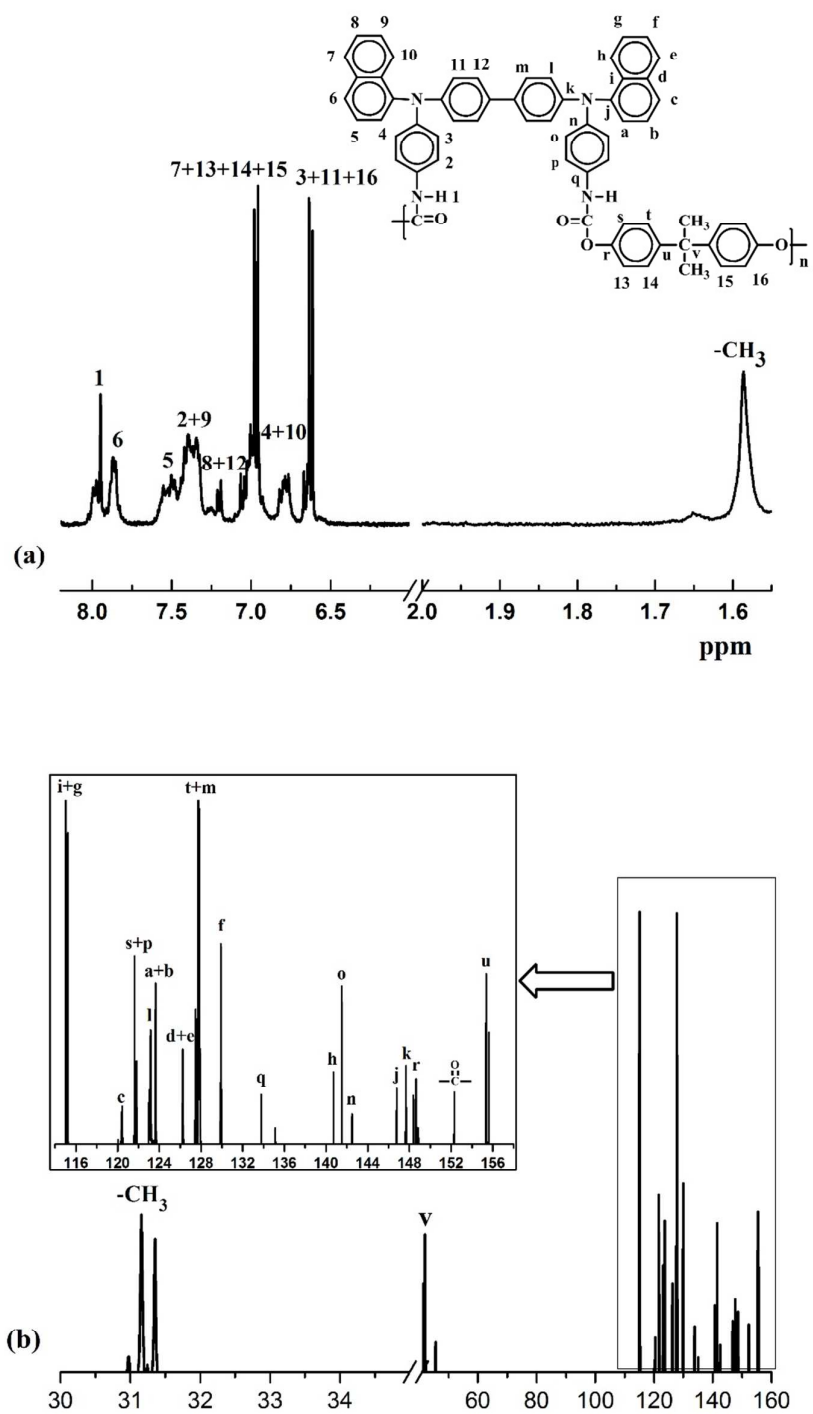
top electrode.

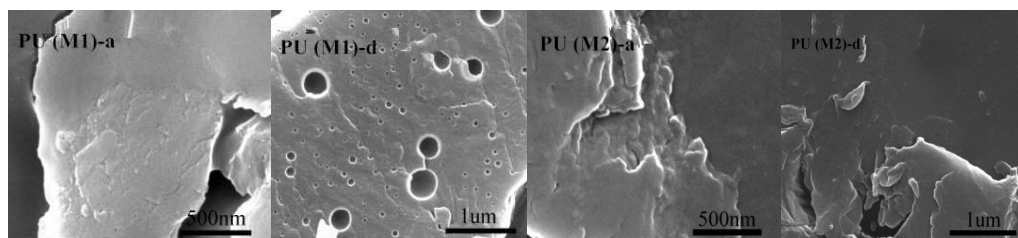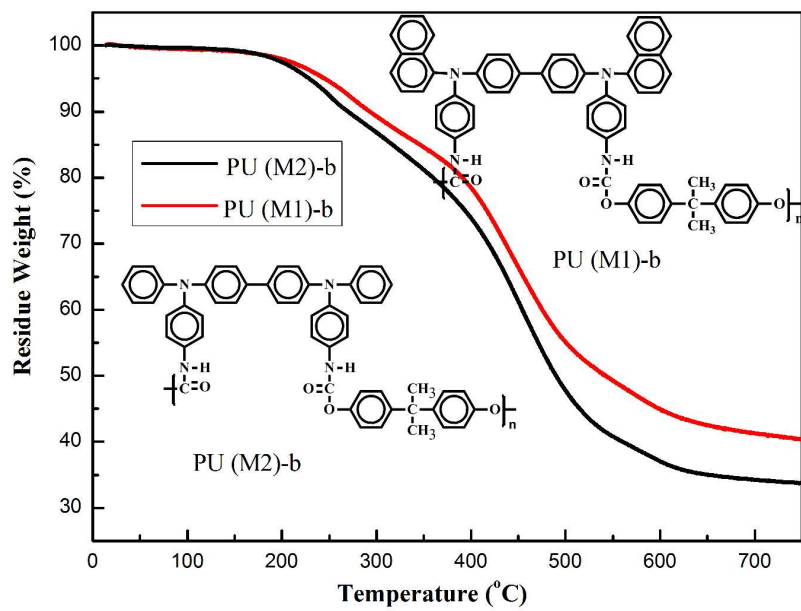**Fig. 2** ^{1}H and ^{13}C NMR spectra of PU (M1)-b in DMSO-d[6].

Fig. 3 SEM images of PU (M1)-a, PU (M1)-d and PU (M2)-a, PU (M2)-d.

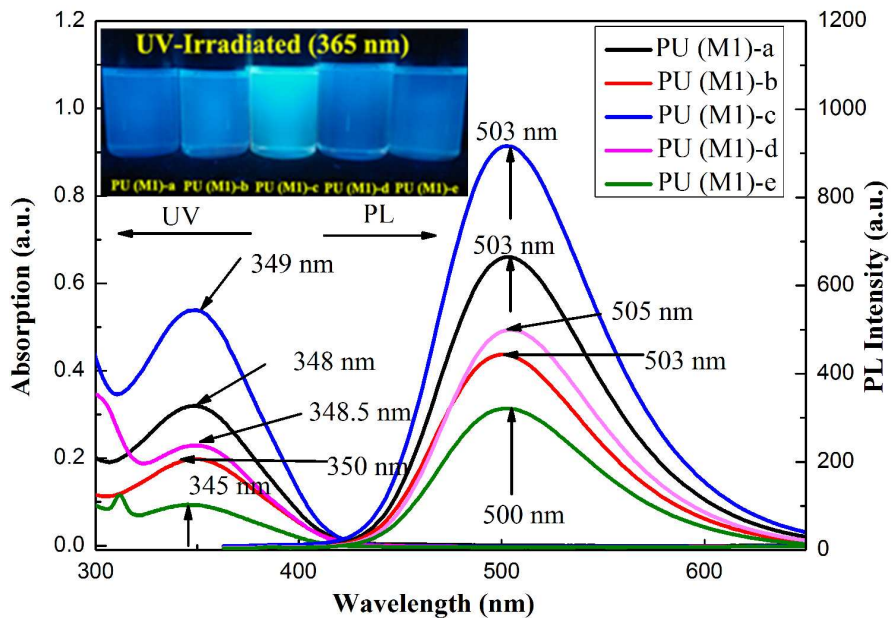**Fig. 4** TGA thermograms of PU (M1)-b and PU (M2)-b at a scan rate of 10 ^{o}C/min.

Fig. 5 UV-vis absorption and PL spectra of PUs (M1) with a concentration of DMSO (conc.: 10^{-8}

M). PL photos of PUs in DMSO solution (10^{-8} M) by UV irradiation (Excited at 365 nm) being
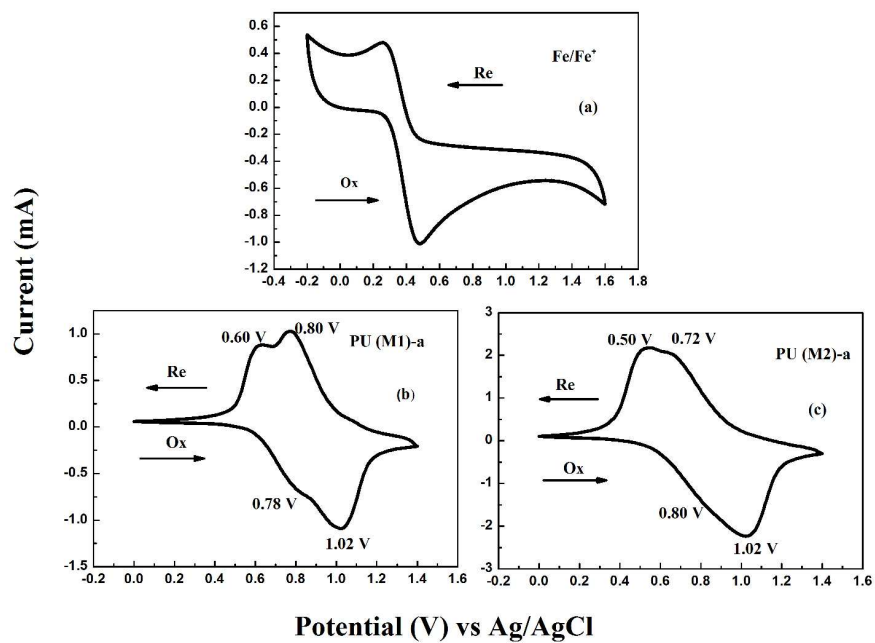
inset).

Fig. 6 CVs of (a) ferrocene (b) PU (M1)-a (c) PU (M2)-a films onto an ITO-coated glass substrate

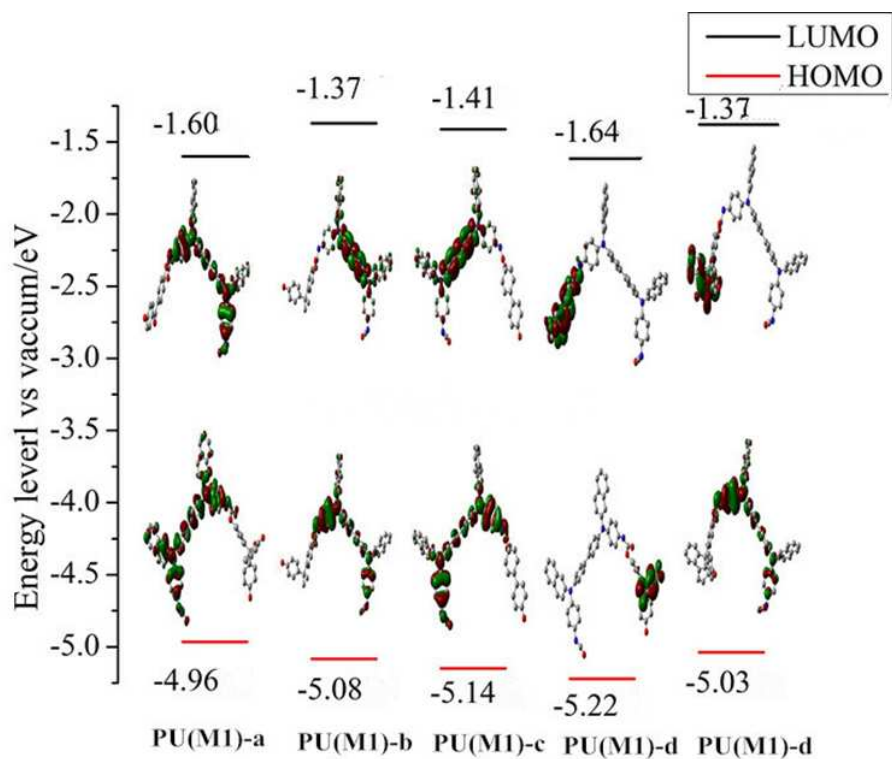in 0.1 M LiClO$_4$/CH$_3$CN at the scanning rate of 50 mV/s.

Fig. 7 Pictorial representations of the electron density in the frontier molecular orbitals of
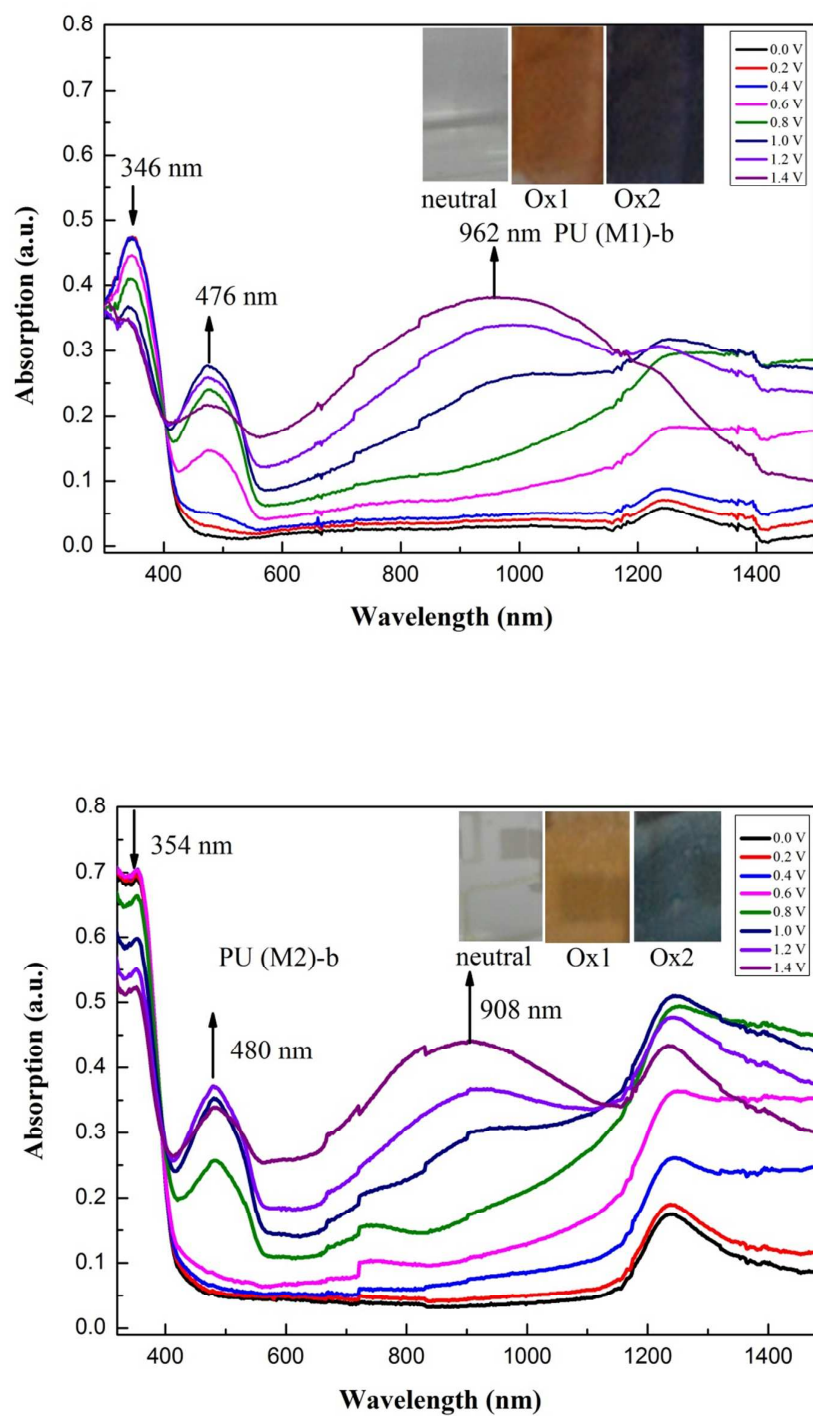
repetition units for PUs (M1).

Fig. 8 Electrochromic behaviors of PU (M1)-b and PU (M2)-b thin film (in CH_3CN with 0.1 M $LiCO_4$ as the supporting electrolyte) at 0.0 V to 1.40 V (insets are the pictures of oxidized PU (M1)-b and PU (M2)-b).
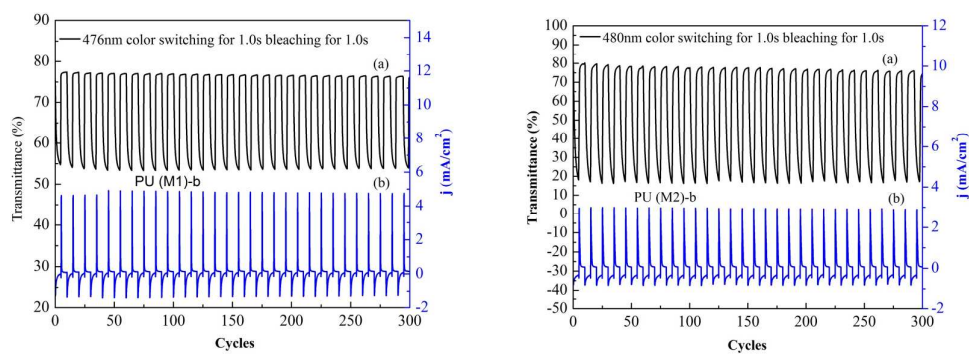
Fig. 9 Optical switching procedures (0.1 M LiClO$_4$ as the supporting electrolyte with a cycle time of 10 s): (a) potential step transmittance and (b) Current consumption of PU (M1)-b and PU (M2)-b at 480 nm.
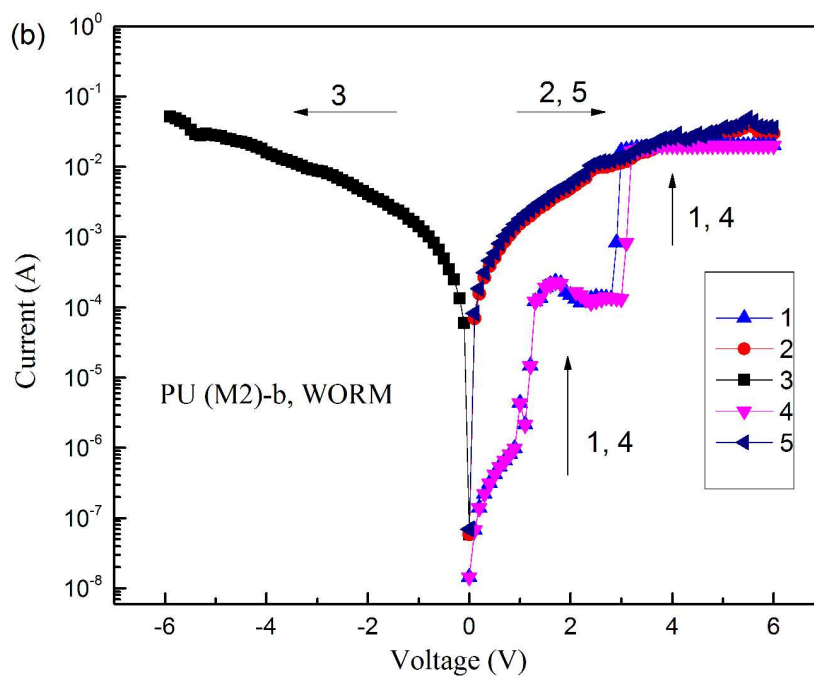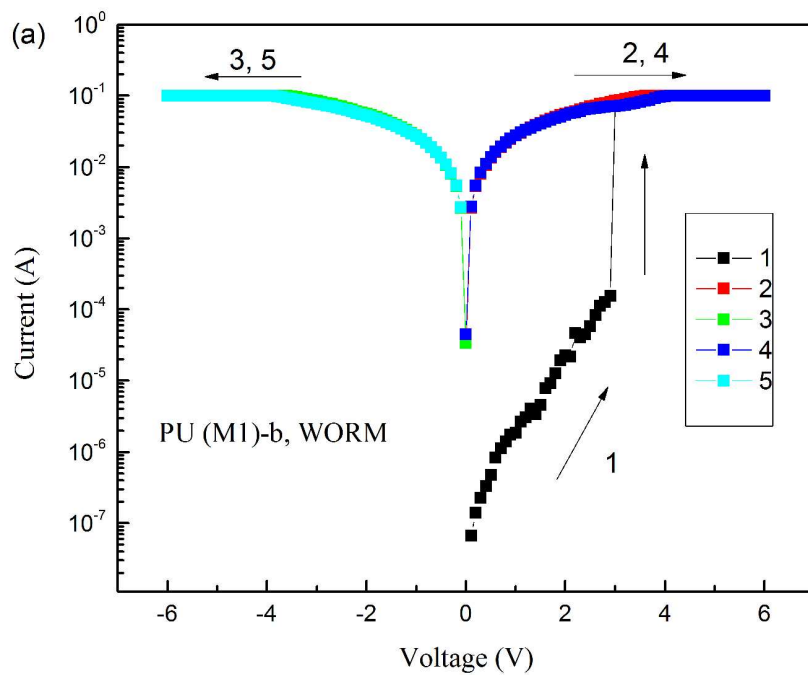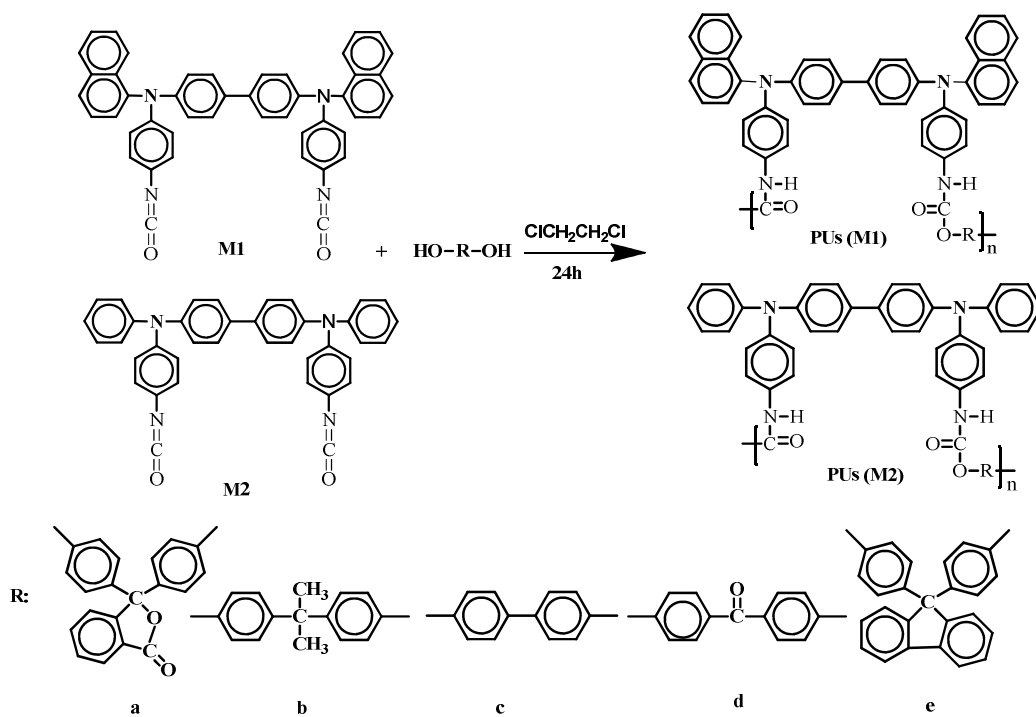
Fig. 10 Curent-voltage (I-V) characteristics of the ITO/polymer (50nm)/Al memory device. (a) PU (M1)-b, (b) PU (M2)-b.

Scheme1 Synthesis routes of PUs.

Table 1 Optical and electrochemical properties of the PUs.

	λ_{film}^{abs}	λ_{onset}^{abs}	$E_{1/2}$vs	E_{onset}^{peak}vs	$E_{HOMO}^{electro}$	$E_{LUMO}^{electro}$	E_g^{film}	E_{HOMO}^{quntum}	E_{LUMO}^{quntum}	E_g^{quntum}
	(nm)[a]	(nm)[b]	Ag/AgCl[c]	Ag/AgCl	(eV)[d]	(eV)[d]	(eV)[d]	(eV)[e]	(eV)[e]	(eV)[e]
PU(M1)-a	480	552	0.69/0.91	0.59	-5.02	-2.77	2.25	-4.96	-1.60	3.36
PU(M1)-b	476	554	0.70/0.90	0.59	-5.02	-2.78	2.24	-5.08	-1.37	3.71
PU(M1)-c	476	552	0.71/0.90	0.60	-5.03	-2.78	2.25	-5.14	-1.41	3.73
PU(M1)-d	480	554	0.71/0.89	0.59	-5.02	-2.78	2.24	-5.22	-1.64	3.57
PU(M1)-e	478	549	0.69/0.89	0.60	-5.03	-2.77	2.26	-5.04	-1.37	3.66
PU(M2)-a	480	561	0.65/0.87	0.54	-4.99	-2.78	2.21	-4.85	-1.62	3.23
PU(M2)-b	480	554	0.72/0.85	0.63	-5.06	-2.82	2.24	-5.04	-1.34	3.70
PU(M2)-c	480	554	0.70/0.84	0.60	-5.03	-2.79	2.24	-5.13	-1.37	3.75
PU(M2)-d	480	552	0.73/0.85	0.64	-5.07	-2.82	2.25	-5.12	-1.90	3.22
PU(M2)-e	484	553	0.68/0.84	0.59	-5.02	-2.78	2.24	-5.00	-1.43	3.57

a UV-vis absorption of the polymer film.

b λ_{onset} of the polymer film.

c $E_{1/2}$: average potential of the redox couple peaks.

d The measured data of the polymers.

e Theoretical calculation of the polymers.